ORIGINAL ARTICLE

GPS observations of the ionospheric F2-layer behavior during the 20th November 2003 geomagnetic storm over South Korea

Shuanggen Jin · O. F. Luo · P. Park

Abstract The ionospheric F2-layer peak density (NmF2) and its height (hmF2) are of great influence on the shape of the ionospheric electron density profile Ne (h) and may be indicative of other physical processes within the ionosphere, especially those due to geomagnetic storms. Such parameters are often estimated using models such as the semiempirical international reference ionosphere (IRI) models or are measured using moderately priced to expensive instrumentation, such as ionosondes or incoherent scatter radars. Global positioning system (GPS) observations have become a powerful tool for mapping high-resolution ionospheric structures, which can be used to study the ionospheric response to geomagnetic storms. In this paper, we describe how 3-D ionospheric electron density profiles were produced from data of the dense permanent Korean GPS network using the tomography reconstruction technique. These profiles are verified by independent ionosonde data. The responses of GPS-derived parameters at the ionospheric F2-layer to the 20th November 2003 geomagnetic storm over South Korea are investigated. A fairly large increase in the electron density at the F2-layer peak (the NmF2) (positive storm) has been observed during this storm, which is accompanied by a significant uplift in the height of the F2 layer peak (the hmF2). This is confirmed by independent ionosonde observations. We suggest that the F2-layer peak height uplift and NmF2 increase are mainly associated with a strong eastward electric field, and are not associated with the increase of the O/N_2 ratio obtained from the GUVI instruments aboard the TIMED satellite. It is also inferred that the increase in NmF2 is not caused by the changes in neutral composition, but is related to other nonchemical effects, such as dynamical changes of vertical ion motions induced by winds and $E \times B$ drifts, tides and waves in the mesosphere/lower thermosphere region, which can be dynamically coupled upward to generate ionospheric perturbations and oscillations.

Keywords GPS · Ionosphere · F2-layer · Tomography · Geomagnetic storm

S.G. Jin (✉) · O. F. Luo · P. Park
Korea Astronomy and Space Science Institute,
Daejeon 305-348, South Korea
e-mail: sgjin@kasi.re.kr; sg.jin@yahoo.com

S.G. Jin
Royal Observatory of Belgium, Brussels 1180, Belgium
e-mail: shuanggen.jin@gmail.com

1 Introduction

It is well known that geomagnetic storms may profoundly affect the global ionosphere and upper atmosphere, inducing great variations in parameters such as the total electron content (TEC), the F2-layer peak density (NmF2) and its height (hmF2). These influences vary with location, season, local time and solar activity. The responses of the ionosphere to geomagnetic storms have been studied for several decades using moderately priced to expensive instrumentation, such as ionosondes and incoherent scatter radar (ISR) (Fuller-Rowell et al. 1996; Szuszczewicz et al. 1998; Lei et al. 2004). However, it is well known that ionospheric storms have a global impact on ionization, and under very disturbed conditions, the ionospheric response to severe storms often presents significant changes in the distribution of ionization with latitude and altitude. Furthermore, ionosondes cannot measure the topside ionosphere and sometimes suffer from absorption during storms, whereas ISRs have geographical limitations. Nowadays, the global positioning system (GPS) satellites, being in high altitude orbits (∼20,200 km), are very useful for studying the structure of the entire ionosphere, even

the plasmasphere. Moreover, GPS is a low-cost, all-weather, near real time and high-resolution atmospheric sounding technique. Therefore, GPS has been widely used to monitor the ionosphere (e.g., Afraimovich et al. 2000; Yamamoto et al. 2000; Gao and Liu 2002; Yin et al. 2004).

As the F2-layer peak electron density value (denoted as NmF2, proportional to the square of the F2 layer critical frequency foF2) is of great influence on the shape of the ionospheric electron density profile Ne(h), and also probably related to various physical processes of ionospheric activities as well as the F2-layer peak height (hmF2), the NmF2 and hmF2 are essential parameters for monitoring ionospheric activities and understanding the nature of the ionosphere. Although many studies of geomagnetic storms have been carried out in United states and Europe (e.g., Foster et al. 2002, 2004; Yin et al. 2004; Goncharenko et al. 2007), investigations on ionospheric behavior to storms in Asia are relatively few due to a lack of dense sets of GPS observations, etc. In this paper, the responses of the GPS-derived NmF2 and hmF2 to the super geomagnetic storm (20 November 2003) over South Korea are described using the data from the dense Korean GPS network (KGN). First, ground-based dual-frequency GPS observations are used to produce electron density profiles using the ionospheric tomography technique, which are verified by independent ionosonde data. Then the responses of the key ionospheric F2-layer parameters NmF2 and hmF2 to the 20th November 2003 geomagnetic storm over South Korea are investigated to gain insights into the effects of different physical conditions and processes.

In addition, the global neutral atmosphere was simultaneously monitored by the TIMED spacecraft in a 625-km circular orbit above the Earth. The global ultraviolet imager (GUVI) instrument onboard the spacecraft produces far-ultraviolet imaging spectrograms of photons emitted from the upper atmosphere, providing neutral composition information (see, e.g., Christensen et al. 2003). The observations from the TIMED/GUVI instrument provide possible mechanisms of the ionospheric behavior to this geomagnetic storm and other solar activity indices as well.

2 Data and tomography method

2.1 GPS observation data

The KGN consists of more than 50 permanent GPS sites (Fig. 1) that have been established since 2000 by the Korea Astronomy and Space Science Institute (KASI), the Ministry Of Governmental Administration and Home Affairs (MOGAHA), and the National Geographic Information Institute (NGI) (Jin and Park 2006). The average distance between GPS sites is about 20–50 km, which provides high spatial
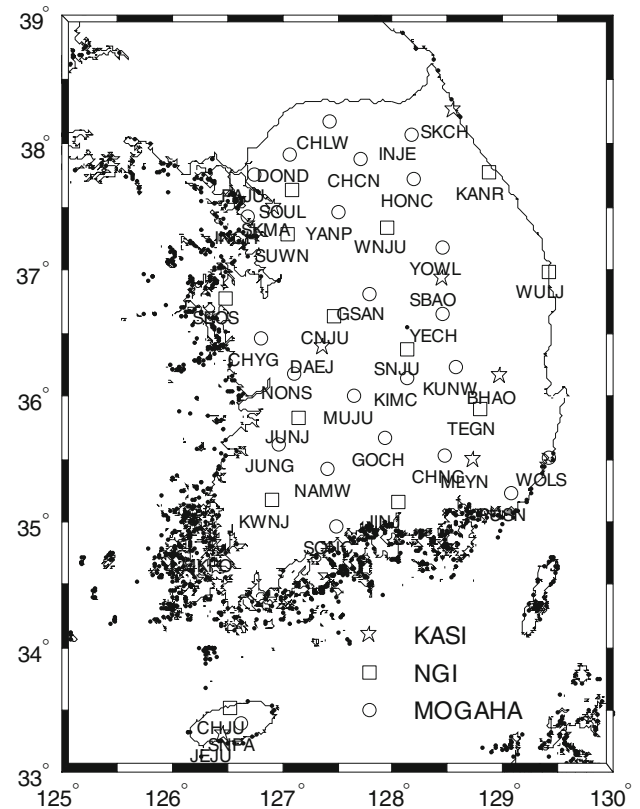
Fig. 1 GPS site distribution of the permanent Korean GPS network (KGN). GPS stations marked by *stars* are operated by the Korea Astronomy and Space Science Institute (KASI); GPS stations marked by *squares* are operated by the National Geographic Information Institute (NGI); GPS stations marked by *circles* are operated by the Ministry of Governmental Administration and the Home Affairs (MOGAHA)

resolution coverage. These dense GPS observations can be used to compute daily station positions, precipitable water vapor (PWV) and TEC, which offer opportunities to investigate crustal deformation, climate and space environments over the southern Korean Peninsula. For this study, the ground-based GPS observations of the KGN network are used to produce 3D (latitude–longitude–height) ionospheric electron density profiles over South Korea and to study the behavior of the ionospheric F2-layer during the 20th November 2003 storm.

2.2 GPS ionospheric tomography method

The GPS consists of a constellation of up to 30 operating satellites in six circular orbits 20,200 km above the Earth at an inclination angle of 55° with a 12-h (sidereal) period. Each GPS satellite broadcasts two spread spectrum L-band radio signals with the frequencies $f_1 = 1.57542\,\text{GHz}$ and $f_2 = 1.2276\,\text{GHz}$. As the ionosphere is a dispersive medium, dual-frequency GPS receivers are able to evaluate the ionospheric effect by measuring the modulations on the codes

and the carrier phases. The equations of carrier phase (L) and code observations (pseudorange P) of dual-frequency GPS are expressed as follows:

$$
\begin{aligned}
L_{k,j}^i = \lambda_k \phi_{k,j}^i &= \rho_{0,j}^i - d_{\mathrm{ion},k,j}^i + d_{\mathrm{trop},j}^i + c\left(\tau^i - \tau_j\right) \\
&\quad - \lambda_k \left(b_{k,j}^i + N_{k,j}^i\right)
\end{aligned}
$$

$$
\begin{aligned}
P_{k,j}^i &= \rho_{0,j}^i + d_{\mathrm{ion},k,j}^i + d_{\mathrm{trop},j}^i + c\left(\tau^i - \tau_j\right) \\
&\quad + d_{q,k}^i + d_{q,k,j}^i + \varepsilon_j^i
\end{aligned}
\tag{1}
$$

where subscript k stands for the frequency ($k = 1, 2$), superscript i and subscript j represent the satellite and ground-based GPS receiver, respectively, and other parameters are as follows:

ρ_0, the true distance between the GPS receiver and satellite
d_{ion} and d_{trop}, the ionospheric and tropospheric delays
c, the speed of light in vacuum space
τ, the satellite or receiver clock offset
b, the phase delay of satellite and receiver instrument bias
d_q, the code delay of satellite and receiver instrument bias
λ, the carrier wavelength
ϕ, the total carrier phase between the satellite and receiver
N, the ambiguity of the carrier phase
ε, other residuals

One can easily obtain the following equations from Eq. 1:

$$
L_4 = L_{1,j}^i - L_{2,j}^i = -40.3\left(\frac{1}{f_1^2} - \frac{1}{f_2^2}\right)\mathrm{STEC} + B_4 \tag{2}
$$

$$
P_4 = P_{1,j}^i - P_{2,j}^i = 40.3\left(\frac{1}{f_1^2} - \frac{1}{f_2^2}\right)\mathrm{STEC} + b_4 \tag{3}
$$

where STEC is the slant TEC of the GPS signal ray path, ($B_4 = -\lambda_1(b_{1,j}^i + N_{1,j}^i) + \lambda_2(b_{2,j}^i + N_{2,j}^i)$), and $b_4 = (dq_{1,j} - dq_{2,j}) + (dq_1^i - dq_2^i)$. The differential code biases (b_4) can be estimated as constant values for each day from GPS carrier phase observations (the detailed processes are described by, e.g., Sardon et al. 1994), and B_4 can be obtained as $\sum_{i=1}^{N}(P_4 + L_4 - b_4)/N$, where N is the number of samples for one arc of GPS observations. Thus, the precise STEC can be derived from dual-frequency GPS carrier phase and code observations (Jin et al. 2004, 2006). The STEC is defined as the line integral of the electron density which is as expressed as follows:

$$
\mathrm{STEC} = \int_{R_{\mathrm{receiver}}}^{R_{\mathrm{satellite}}} N_e\left(\lambda, \varphi, h\right)\,\mathrm{d}s \tag{4}
$$

where $N_e(\lambda, \varphi, h)$ is the ionospheric electron density; λ, φ and h are the longitude, latitude and height, respectively. To obtain N_e, the ionosphere is divided into grid pixels with a small cell, where the electron density is assumed to be constant, so that the STEC in Eq. 4 along the ray path i can be approximately written as a finite sum over the pixels j as follows:

$$
\mathrm{STEC}_i = \sum_{j=1}^{M} a_{ij} n_j \tag{5}
$$

where a_{ij} is a matrix whose elements denote the length of the path–pixel intersections in the pixel j along the ray path i, and n_j is the electron density for the pixel j. Each set of STEC measurements along the ray paths from all observable satellites at consecutive epochs are combined with the ray path geometry into a linear expression:

$$
Y = Ax + \varepsilon \tag{6}
$$

where Y is a column of m measurements of STEC, x is a column of n unknown electron densities for cells in the targeted ionosphere region and A is an $m \times n$ normal matrix with elements a_{ij}. The unknown electron densities x can be estimated by the ionospheric tomographic reconstruction technique. Many tomography algorithms are used in different ways, e.g., singular value decomposition (Wall et al. 2001), correlation function (Ruffini et al. 1998) and algebraic reconstruction technique (ART; Gordon et al. 1970). One of the most common approaches is the ART, which was first introduced in computerized ionospheric tomography (CIT) by Austen et al. (1988). This is an iterative procedure for solving a linear equation. A modified version of ART is the so-called multiplicative ART (MART), where the correction in each iteration is obtained by making a multiplicative modification to x (Raymund et al. 1990; Tsai et al. 2002). The ART generally produces estimates of the unknown parameters by minimization of the L2 norm, while the MART follows maximum entropy criteria and thus underlies different statistics. In addition, the MART performs a multiplicative modification in each iteration, and thus the inversion results are always positive. Therefore, MART has the advantage over ART in determining the electron densities that avoid unreasonable negative values and is the one used in this study. Basically, the MART algorithm is iterated cyclically:

$$
x_j^{k+1} = x_j^k \left(\frac{y_i}{\langle a_i, x^k \rangle}\right)^{\lambda_k a_{ij}} \tag{7}
$$

where y_i is the ith observed STEC in a column of m measurements, x_j is the jth resulted cell electron density in a column of n unknowns, a_{ij} is the length of link i that lies in cell j, λ_k is the relaxation parameter at the kth iteration with $0 < \lambda_k < 1$ and the inner product of the vectors x and a_i is the simulated STEC for the ith path. The electron density matrix x is therefore corrected iteratively by the ratio of the measured STEC and the simulated STEC with a relaxation parameter of λ_k

Fig. 2 Flow chart of MART

Fig. 3 Comparison of the electron density profiles derived from the ground-based GPS tomography reconstruction (*solid line*), ionosonde observation at Anyang stations (37.39°N, 126.95°E) (*dot line*) and IRI-2007 estimation (*dashed line*) at 9:00 UT on 1st October 2003
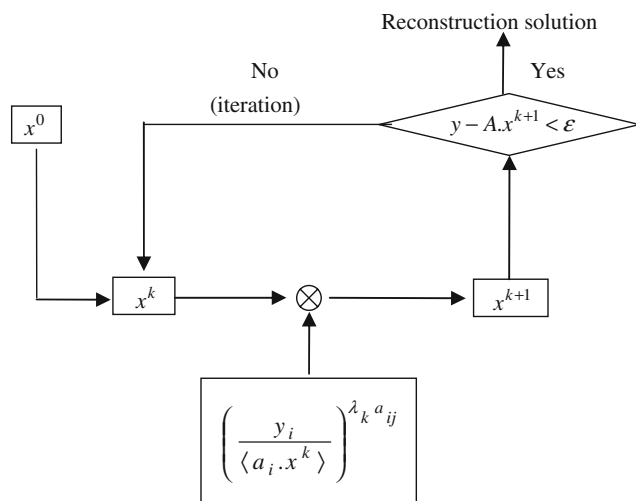
until the residual does not change (see Fig. 2). This relaxation parameter value is chosen from the experience in which the best λ_k value is identified, where the solution converges quickly with a reasonable number of iterations and the residuals are a minimum. Here, $\lambda_k = 0.01$ has been chosen for all iterations. In addition, it is noted that any iterative algorithm requires an initial condition before the iteration begins. Because of the poor STEC geometry, the initialization could be extremely important for the tomographic reconstruction. In practice, the closer the initial condition is to the true electron density distribution, the more accurate the reconstruction will be. Here, the latest IRI-2007 model (http://nssdcftp.gsfc.nasa.gov/models/ionospheric/iri/iri2007) is used as an initial guess for the reconstruction iteration.

2.3 Reliability of GPS ionospheric tomography

The ionospheric reconstruction algorithm MART can integrate the STEC from all available GPS receivers to all GPS satellites visible from each site of the KGN network above a user-specified elevation cut-off angle (usually 15°). The unknown electron density profile is expressed in 4D (longitude–latitude–height and time) voxel basis functions over the following grid: longitude 124°E–130°E in 1°-increments, latitude 33°N–39°N in 0.5°-increments, altitude 100–1,000 km in 25-km increments and 1-h increments in time of linear change in the electron density per voxel. As there are a sparse number of ions in the ionosphere above 1,000 km, the effect on the inversion for ionospheric electron density profiles is very small and the ionosphere is only considered up to an altitude of 1,000 km. Furthermore, it is faster to invert the unknown ionospheric density parameters due to the reduced number of unknown variables. In addition, the fewer leaving rays from the ionospheric space of above-defined latitude and longitude range are not used, but are
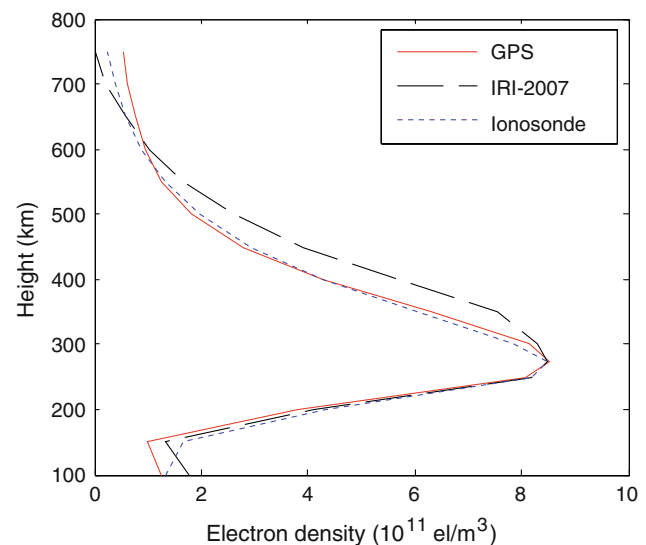
useful to further obtain ionospheric profiles outside the latitudinal/longitudinal boundary space. Using the STEC of all ray paths passing the ionospheric grid cells from the KGN, the 4D ionospheric electron density profiles can be derived through the tomography reconstruction algorithm. To verify the reliability of GPS ionospheric tomography reconstruction results, the available ionosonde station (Anyang) in South Korea provides an independent comparison with the GPS tomographically reconstructed electron density profiles. The electron density profiles at 25-km height steps from GPS reconstruction and ionosonde data match well in October and November with a root-mean-square (RMS) of 0.3×10^{11} electrons/m^3. For example, Fig. 3 shows a comparison of the GPS reconstructed electron density profile at 9:00 UT on 1st October 2003 with the available ionosonde data at Anyang station (37.39°N, 126.95°E) and the profiles from the IRI-2007 model. It can be seen that the GPS tomographically reconstructed density profile is in good agreement with the ionosonde data and the IRI-2007 model, but is closer to the ionosonde, which confirms the validity of our GPS ionospheric reconstruction approach (Jin et al. 2007). Figures 5, 6 and 7 also show that our GPS reconstructed electron density profiles agree well with the independent ionosonde observations during the storm time.

3 Results and discussions

3.1 Geomagnetic conditions

A strong geomagnetic storm commenced on 20th November 2003, as confirmed by the Dst index time series in Fig. 4
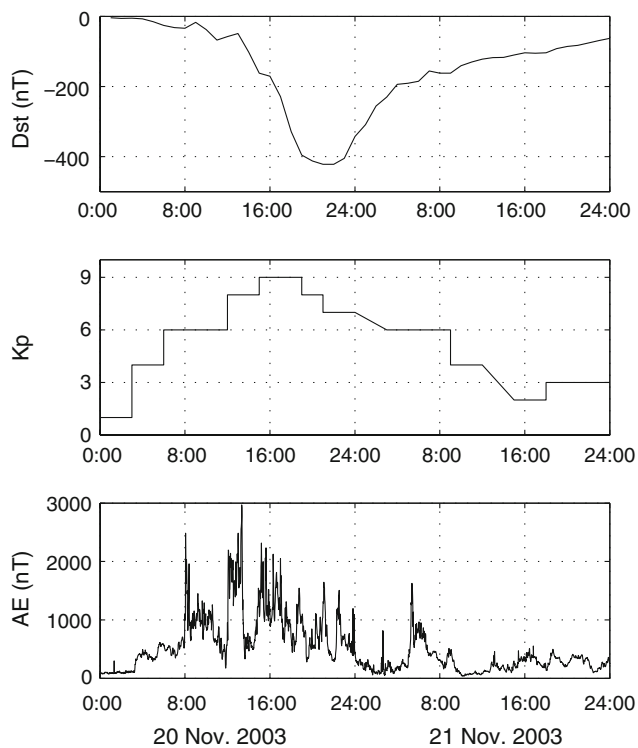
Fig. 4 The geomagnetic storm index (Dst) (*upper*), K_p (*middle*) and AE indices (*bottom*) on 20–21 November 2003
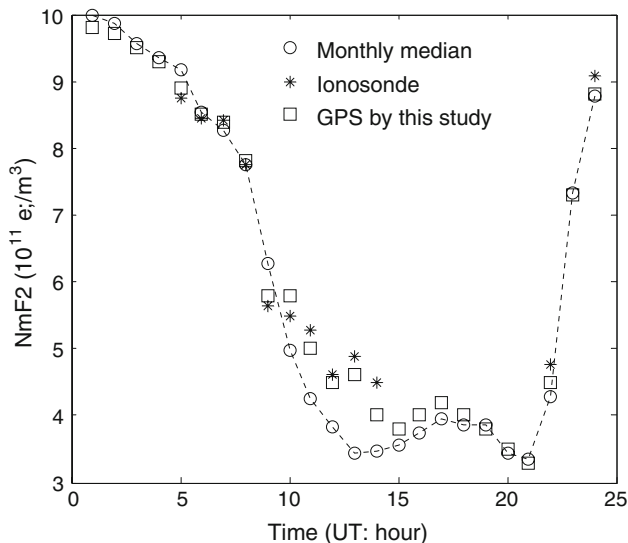
Fig. 5 Comparison of F2-layer peak densities (NmF2) from the monthly median, ionosonde and GPS observations on 20th November 2003

obtained from the World Data Center in Kyoto (http://swdcdb.kugi.kyoto-u.ac.jp/). The Dst or disturbance storm time index in nanoteslas (nT) is a measure of geomagnetic activity used to assess the severity of magnetic storms based on the average value of the horizontal component of the Earth's magnetic field measured hourly at four near-equatorial geomagnetic
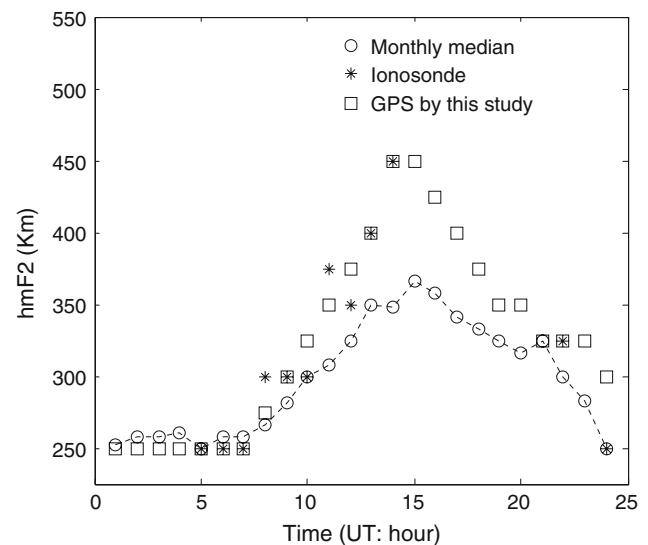
Fig. 6 Comparison of F2-layer peak heights (hmF2) from the monthly median, ionosonde and GPS observations on 20th November 2003

observatories. The storm started with the arrival of the shock at about 8:00 UT on 20th November 2003 and reached a minimum Dst value of −472 nT at 20:00 UT, accompanied with an AE index up to 2,600 nT and a maximum Planetary K-index (K_p) value of nine at about 16:00 UT. Here, the AE index is the auroral electrojet index obtained from a number of stations distributed in local time in the latitude region that is typical of the northern hemisphere auroral zone, which provides a measure of the overall horizontal current strength. The planetary K-index (K_p) is a disturbed level of geomagnetic field, which can be obtained from a number of magnetometer stations at mid-latitudes. As can be seen from these indices, the magnetic activity returned to normal level by 22nd November 2003.

3.2 Disturbance of GPS observed F2-layer parameters

As the F2-layer peak electron density (NmF2) and its height (hmF2) are of great influence on the shape of the ionospheric electron density profile Ne (h), the NmF2 and hmF2 are key parameters for monitoring ionospheric conditions to understand the nature of ionospheric activities. Therefore, the behavior of the ionospheric F2-layer was investigated in detail over South Korea in terms of the NmF2 and hmF2 during the geomagnetic storm (20 November 2003). The peak density (NmF2) and its corresponding height (hmF2) can be easily obtained from the ground-based GPS reconstructed results of electron density profiles with the ionospheric height. By checking the solar geophysical index series (Dst, K_p and AE) from the World Data Center in Kyoto in November 2003, the days 1–19 and 22–30 of November are magnetically quiet. The monthly median value of electron

Fig. 7 Comparison of the GPS and Ionosonde observations and monthly median from GPS-derived electron density profiles at 13:00 UT on 20th and 23rd November 2003. (Note: only values at 50-km height step are plotted, for better readability)
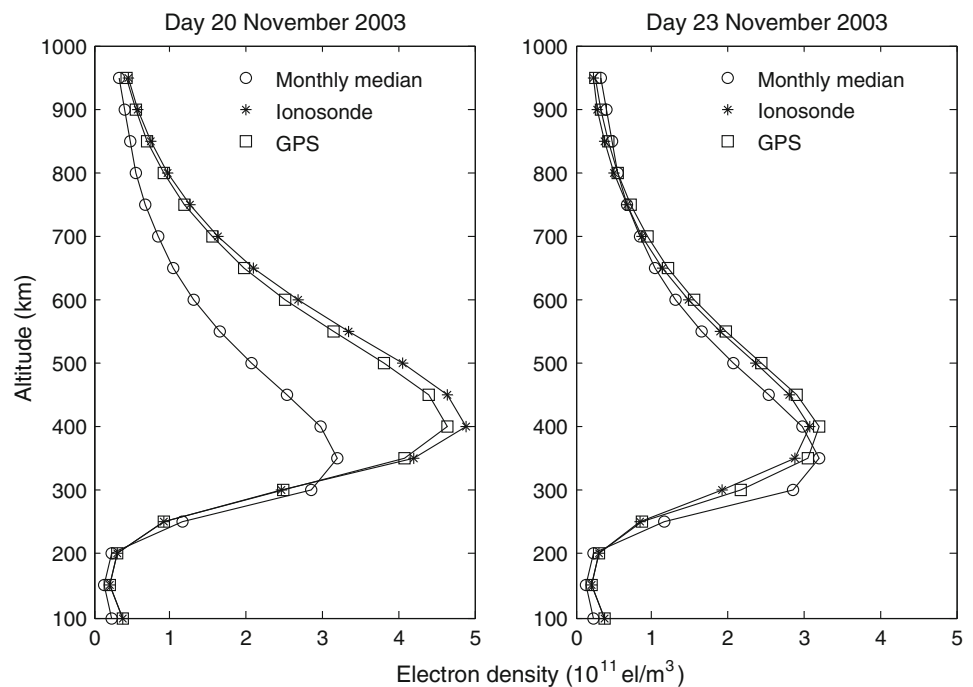
density profiles during these quiet days is taken as the reference and the deviation can be regarded as the variation of ionospheric F2 peak density and height during the geomagnetic storm.

Figures 5 and 6 show the NmF2 and hmF2 hourly time series of monthly median, ionosonde data and GPS observations at the grid site (37.5°N, 127.0°E) on 20th November 2003, where the monthly median is calculated from one month of GPS-derived electron density profiles. It can be seen that there are anomalous variations during this storm, which is also confirmed by independent ionosonde observations at Anyang station. Some ionosonde results are blank, as it cannot measure the ionosphere due to suffering from absorption during this storm. The GPS-derived F2-layer peak density (NmF2) has an anomalous change at 9:00 UT and increases from 10:00 UT until 19:00 UT. The F2-layer peak height (hmF2) suddenly rises from 8:00 UT when the shock of this storm just started, and reaches the maximum height at about 16:00 UT with a maximum K_p value of nine, and then gradually descends until 21:00 UT. The significant increases of F2-layer peak height and density last for about 10 h and is classified as a long-duration ionospheric positive storm (Huang et al. 2005a). The electron density profile comparison also shows the same enhancements of the F2-region from 10:00 UT to 19:00 UT. For example, Fig. 7 is a comparison of electron density profiles between the GPS, ionosonde data and monthly median at 13:00 UT. It can be clearly seen that the electron density profiles are significantly increased above the F region on 20th November 2003, especially the NmF2, which increased by about 45% accompanied by a significant uplift in the height of the F2 layer peak (the hmF2), while

on the quiet day (23 November 2003) the electron density profiles are almost close to the monthly median value. In addition, the responses of the NmF2 and hmF2 to this storm at different latitudes (i.e. different grid sites) were analyzed, and almost similar results were obtained, which is mainly due to the small area of South Korea. As the TEC is the integrated electron density along a path through the ionosphere (Eq. 4), the TEC variations over South Korea during this storm are similar to the NmF2 behavior.

3.3 Variations in thermospheric composition

It is well known that in the F region the increase/loss rate of electron density depends mainly on the molecular nitrogen concentration $[N_2]$ with some contribution from molecular oxygen concentration $[O_2]$, while the production rate depends on the atomic oxygen concentration $[O]$. Other mechanisms (meridional winds, electric fields) also lead to redistribution of electron density in height as they move plasma up or down the field lines. To describe changes in the thermospheric composition, the experimental data of the O/N_2 column density obtained by the GUVI instrument on board the TIMED satellite is used. The GUVI column O/N_2 ratio is determined from the O (135.6 nm) and N_2 (LBH) emissions (Strickland et al. 1995, 2004; Christensen et al. 2003) and is estimated with $1.75° \times 1.75°$ spatial resolution (detailed discussions of the definition of O/N_2 column density ratio and the analysis technique can be found in the earlier-referenced papers). The estimated errors in O/N_2 may reach ~10% for high O/N_2 values and latitudes above 60°,
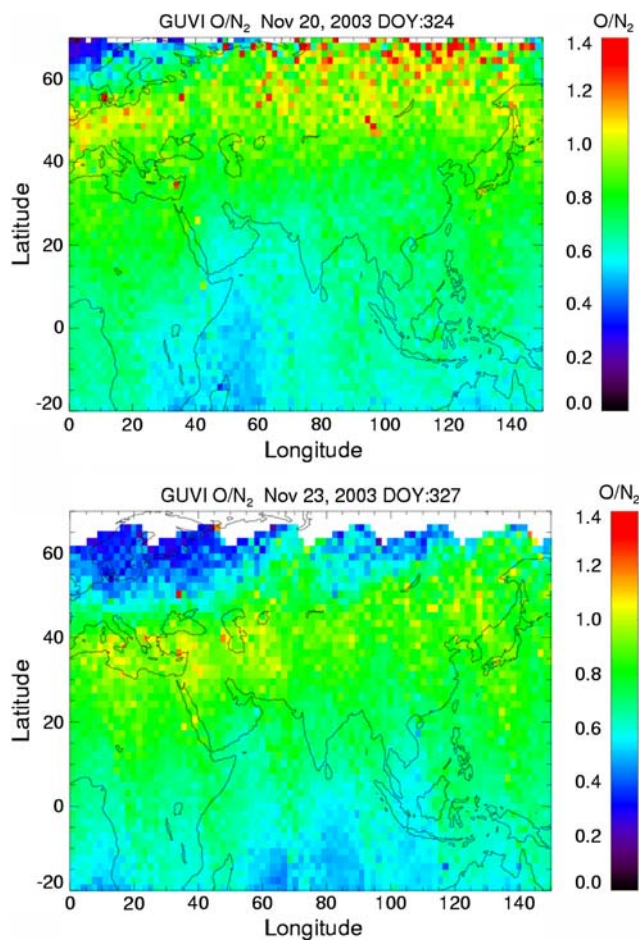
Fig. 8 GUVI O/N$_2$ ratios on 20th and 23rd November 2003. The data were recorded around 12:00 UT for longitudes 0°–150°E and latitudes 20S°–60°N

but are expected to be close to 5% for low O/N$_2$ values as well as at lower latitudes. Although some questions about absolute O/N$_2$ values still need to be resolved due to uncertainties in cross sections, relative variations in O/N$_2$ ratio should not be affected, as discussed by Christensen et al. (2003) and Strickland et al. (2004).

Figure 8 presents the O/N$_2$ ratio in the range of 0°–150°E and 20S°–60°N on the storm day (20 November 2003) and on the quiet day (23 November 2003). The distinctive feature of the measurements is a large latitudinal gradient of O/N$_2$ in high latitude regions on 20th November 2003 and lower values at high latitudes on the quiet day (23 November 2003). It illustrates that the transition from equinox to solstice thermospheric circulation is already well underway. Furthermore, during the quiet time on day 23, the O/N$_2$ ratio is decreased near the magnetic poles, indicating sensitivity of thermospheric composition to high latitude heating. Generally speaking, the variations in neutral composition (O/N$_2$ ratio) will trigger the increase/loss of ionospheric electron density. Compared with the quiet day (23 November 2003),

the O/N$_2$ ratio on the storm day (20 November 2003) is greatly increased in high latitude Asia and but has no significant change in South Korea, where the increased NmF2 was observed, indicating that the increased NmF2 in South Korea is not caused by changes in neutral composition, and other possible nonchemical effects. Nonchemical causes include dynamical changes of vertical ion motions induced by winds and E×B drifts; e.g., Mendillo et al. (2002) suggested the wind variability effect on the ionospheric variability. Another interesting cause is tides and waves in the mesosphere and lower thermosphere (MLT) region that can be dynamically coupled upward to generate ionospheric perturbations and oscillations (Forbes et al. 1993).

In addition, the phenomenon of F2-layer parameters' responses to the storm is possibly due to the electrodynamics of the F-region. It is known that the shape factor is the most sensitive parameter to the variations of H+/O+ ratio at the F2 peak, or equivalent to the transition level at which [O+]=[H+] (Davies et al. 1976). Large downward fluxes of H+ can decrease the O+ to H+ transition levels, thereby increasing the topside content and hence the F2 peak height. In addition, the variability of F2-layer parameters are quite complex due to their relations to solar and geomagnetic activities or the latitude (Kersley and Hosseinieh 1976; Davies and Liu 1991). Also the NmF2 and hmF2 variability has single day anomalies, day-to-day fluctuations and long-term periodicities of 1 month or more (Bhuyan et al. 1986). Therefore, the F2-layer peak features of the storm need further investigation, with more observations in the future at different locations and solar activity conditions.

3.4 Solar active indices

The electric fields, thermospheric meridian winds, a "composition bulk" and high latitude particle precipitation have been suggested as probable physical mechanisms to explain the ionospheric response to the storm induced disturbances (Fuller-Rowell et al. 1994; Foster 1993; Foster and Vo 2002; Tsurutani et al. 2004). The increase in hmF2 is likely to be associated with a strong eastward electric field and with enhanced equatorward winds relative to quiet periods. A large depletion of ionization results from an increased recombination rate (Buonsanto and Foster 1993). We obtained the helio-geophysical background for the 20th November 2003 storm from several data sources. The interplanetary magnetic field (IMF) data, presented here in geocentric solar magnetospheric system (GSM) coordinates, are obtained from ACE MAG level 2 data, and the solar wind velocity and density are obtained from ACE SWEPAM level 2, both provided by the ACE Science Center (ASC) (http://www.srl. caltech.edu/ACE/ASC/). ACE orbits the L1 libration point, which is a point of Earth-Sun gravitational equilibrium about 1.5 million kilometers from the Earth and 148.5 million
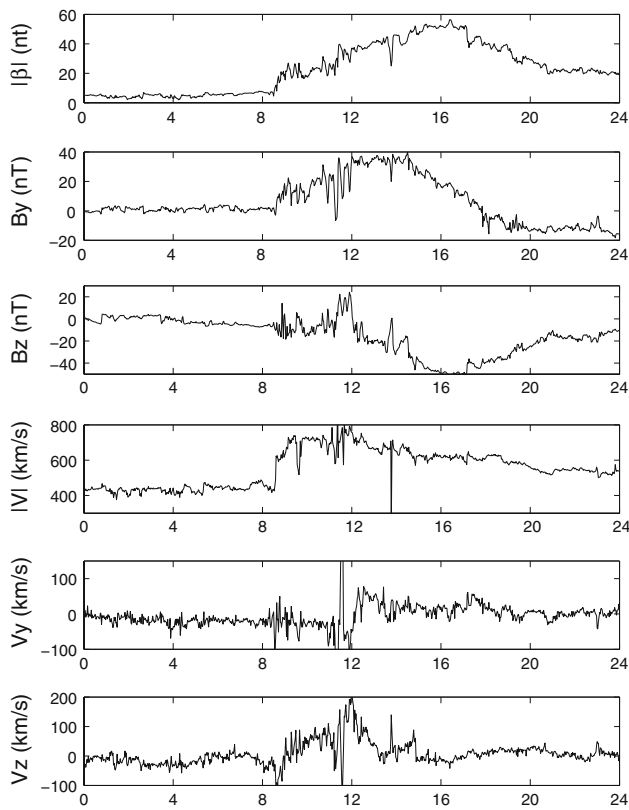
Fig. 9 The magnetic field strength $|\beta|$, y component of IMF (By) and z component of IMF (Bz) and the solar wind parameters (flow speed V, Vy and Vz) on 20th November 2003

kilometers from the Sun. With a semimajor axis of approximately 200,000 km, the elliptical orbit affords ACE a prime view of the Sun and the galactic regions beyond. Proton fluxes and the magnetic field component parallel to the Earth's rotation axis at geostationary orbit distance from the Earth are obtained from GOES-10 satellite data at the Space Environment Center (http://sec.noaa.gov/Data/). The heliogeophysical conditions during the 20th November 2003 storm are depicted in Fig. 9. This figure shows the magnetic field strength and its components in y/z directions and solar wind (SW) parameters. It is noticeable that the Bz component of the IMF displays large variability, starting at about 09:00 UT on 20th November 2003. It rapidly dropped to strongly negative values (reaching a minimum value of about -50 nT), namely enhanced equatorward winds. While the By component of the IMF also displays large variability, starting at about 09:00 UT on 20th November 2003, it rose rapidly to strongly positive values (reaching a maximum value of about 40 nT), indicating a strong eastward electric field. The positive values of the By component are from about 9:00 to 17:00 UT on 20th November 2003. As first suggested by Dungey (1961), the Bz orientation has an important influence on the magnetosphere and high latitude ionosphere, and the more negative Bz is, the more important are the effects on

the ionosphere (Davis et al. 1997), especially arousing the hmF2 rise (Lei et al. 2004). Moreover, an abrupt increase in the SW velocity (from about 450 to 750 km/s) starts at about 09:00 UT on 20th November 2003. These enhancements have lasted for about 8 h, and afterwards the SW velocity returns to typical values of about 500 km/s, whereas SW density displays three additional bursts, the largest one occurring from 9:00 to 16:00 UT on 20th November 2003, especially in the y and z components. These variations with a strong eastward electric field and with enhanced equatorward winds possibly result in uplift of the hmF2 (Goncharenko et al. 2007). Huang et al. (2005a,b) suggested that the enhanced ionospheric electric field is responsible for the generation of the positive storm by moving the F region plasma upward through E×B drifts, and the lower recombination rate at high altitudes will cause a large increase in the F region electron density. A simulation study by Swisdak et al. (2006) confirmed that the electric field played a dominant role on the F region behavior to the storm. In addition, if the entire ionosphere is uplifted, the neutral wind system will be changed as the plasma at low altitude and corresponding ion neutral drag reduce, and the magnetic field will be diffused due to uplifted heavy ions. Therefore, the increase of the F2-layer parameters due to plasma uplift during the storm is possibly one of the most dramatic consequences of magnetosphere–thermosphere–ionosphere coupling (Mannucci et al. 2005).

4 Conclusion

The ionospheric responses to geomagnetic activities as well as its physical mechanisms have been studied over the last three decades using expensive ionosonde and ISR techniques. Some problems, however, are still not well resolved and understood, especially the F2-layer behavior to geomagnetic storms. Nowadays, continuous GPS observations provide an important tool to image the three-dimensional time-evolving ionospheric structure, which can be used to monitor ionospheric behavior during ionospheric activity. In this paper, the responses of the key ionospheric F2-layer parameters (NmF2 and hmF2) to the 20th November 2003 super storm over South Korea have been studied using the GPS ionospheric tomography technique. A strong increase of NmF2 during this storm has been found, accompanied by a significant hmF2 uplift, which is also confirmed by independent ionosonde observations. The uplift of the F2 layer is mainly associated with a strong eastward electric field. The increase of electron density in the F2-layer peak depends mainly on the molecular nitrogen concentration [N_2] with some contribution from molecular oxygen concentration [O_2], while the production rate depends on the atomic oxygen concentration [O]. However, the O/N_2 ratio from the GUVI instrument on board the TIMED satellite shows no significant change

during this geomagnetic storm. It suggests that the increase in NmF2 is not caused by changes in neutral composition, but is related to other possible nonchemical effects, such as dynamical changes of vertical ion motions induced by winds and E×B drifts, tides and waves in the mesosphere/lower thermosphere (MLT) region, which can be dynamically coupled upward to generate ionospheric perturbations and oscillations.

References

Austen JR, Franke SG, Liu CH (1988) Ionospheric imaging using computerized tomography. Radio Sci 23:299–307

Afraimovich E, Kosogorov EA, Leonovich LA (2000) Determining parameters of large scale traveling ionospheric disturbances of auroral origin using GPS arrays. J Atmos Sol Terr Phy 62:553–565

Bhuyan PK, Lakha S, Tyagi TR (1986) Equivalent slab thickness of the ionosphere over 26°N through the ascending half of a solar cycle. Ann Geophys 4:131–136

Buonsanto MJ, Foster JC (1993) Effects of magnetospheric electric fields and neutral winds on the low-middle latitude ionosphere during the March 20–21, 1990, storm. J Geophys Res 98:19133–19140

Christensen AB, Paxton LJ, Avery S, et al (2003) Initial observations with the Global Ultraviolet Imager (GUVI) in the NASATIMED satellite mission. J Geophys Res 108(A12):1451. doi:10.1029/2003JA009918

Davies K, Fritz RB, Gray TB (1976) Measurement of columnar electron contents of the ionosphere and plasmasphere. J Geophys Res 81:2825–2834

Davies K, Liu XM (1991) Ionospheric slab thickness in middle and low-latitudes. Radio Sci 26:997–1005

Davis CJ, Wild MN, Lockwood M, Tulunay YK (1997) Ionospheric and geomagnetic responses to changes in IMF Bz: a superposed epoch study. Ann Geophys 15:217–230

Dungey JW (1961) Interplanetary magnetic field and the auroral zones. Phys Rev Lett 6:47–48

Forbes JM, Roble RG, Fesen CG (1993) Acceleration, heating, and compositional mixing of the thermosphere due to upward propagating tides. J Geophys Res 98:311–321

Foster J (1993) Storm time plasma transport at middle and high latitudes. J Geophys Res 98(A2):1675–1689

Foster J, Erickson P, Coster A, Goldstein J, Rich F (2002) Ionospheric signatures of plasmaspheric tails. Geophys Res Lett 29(13):1623. doi:10.1029/2002GL015067

Foster J, Vo H (2002) Average characteristics and activity dependence of the subauroral polarization stream. J Geophys Res 107(A12):1475

Foster J, Coster A, Erickson P, Rich F, Sandel B (2004) Stormtime observations of the flux of plasmaspheric ions to the dayside cusp/magnetopause, Geophys Res Lett 31:L08809. doi:10.1029/2004GL020082

Fuller-Rowell TJ, Codrescu MV, Moffett RJ, Quegan S (1994) Response of the thermosphere and ionosphere to geomagnetic storms. J Geophys Res 99:3893–3914

Fuller-Rowell TJ, Codrescu MV, Rishbeth H, Moffet RJ, Quegan S (1996) On the seasonal response of the thermosphere and ionosphere to geomagnetic storms. J Geophys Res 101(A2):2343–2353

Gao Y, Liu ZZ (2002) Precise ionosphere modelling using regional GPS network data. J Glob Position Syst 1:18–24

Goncharenko LP, Foster J, Coster A, Huang C, Aponte N, Paxton L (2007) Observations of a positive storm phase on September 10, 2005. J Atmos Solar Terr Phys 69:1253–1272

Gordon R, Bender R, Therman G (1970) Algebraic reconstruction Techniques (ART) for three dimensional electron micoscopy and X-ray photography. J Theor Biol 29:471–481

Huang C, Foster J, Kelley M (2005a) Long duration penetration of the interplentary electric field to the lowlatitude ionosphere during the main phase of magnetic storms. J Geophys Res 110:A11309. doi:10.1029/2005JA011202

Huang C, Foster J, Goncharenko J, Erickson P, Rideout W (2005b) A strong positive phase of ionospheric storms observed by the Millstone Hill incoherent scatter radar and global GPS network. J Geophys Res 110:A06303. doi:10.1029/2004JA010865

Jin SG, Wang JL, Zhang HP, Zhu WY (2004) Real-time monitoring and prediction of the total ionospheric electron content (TEC) by means of GPS. Chin Astron Astrophys 28(3):331–337

Jin SG, Park PH (2006) Strain accumulation in South Korea inferred from GPS measurements. Earth Planets Space 58(5):529–534

Jin SG, Park J, Wang J, Choi B (2006) Electron density profiles derived from ground-based GPS observations. J Navig 59(3):395–401

Jin SG, Park J, Park PH (2007) GPS ionospheric tomography: a comparison with the IRI-2001 model over South Korea. Earth Planets Space 59(4):287–292

Kersley L, Hosseinieh HH (1976) Dependence of ionospheric slab thickness on geomagnetic activity. J Atmos Terr Phys 38:1357–1360

Lei J, Liu L, Wan W, Zhang S (2004) Modeling the behavior of ionosphere above Millstone Hill during the September 21–27, 1998 storm. J Atmos Solar Terr Phys 66:1093–1102

Mannucci A, Tsurutani B, Iijima B, Komjathy A, Saito A, Gonzales W, Guarnieri F, Kozyra J, Skoug R (2005) Dayside global ionospheric response to the major interplanetary events of October 29–30, 2003 "Halloween Storms". Geophys Res Lett 32:L12S02. doi:10.1029/2004GL021467

Mendillo M, Rishbeth H, Roble RG, Wroten J (2002) Modelling F2-layer seasonal trends and day-to-day variability driven by coupling with the lower atmosphere. J Atmos Solar Terr Phys 64:1911–1931

Raymund TD, Austen JR, Franke SJ (1990) Application of computerized tomography to the investigation of ionospheric structures. Radio Sci 25:771–789

Ruffini G, Flores A, Rius A (1998) GPS tomography of the ionospheric electron content with a correlation functional. IEEE Trans Geosci Remote Sens 36(1):143–153

Sardon E, Rius A, Zarraoa N (1994) Estimation of the transmitter and receiver differential biases and the ionospheric total electron content from global positioning system observations. Radio Sci 29(3):577–586

Strickland DJ, Evans JS, Paxton LJ (1995) Satellite remote sensing of thermospheric O/N_2 and solar EUV. 1. Theory. J Geophys Res 100(A7):12217–12226

Strickland DJ, Meier RR, Walterscheid RL, Craven JD, Christensen AB, Paxton LJ, Morrison D, Crowley G (2004) Quiet time seasonal

behaviour of the thermosphere seen in the far ultraviolet dayglow. J Geophys Res 109:A01302. doi:10.1029/2003JA010220

Swisdak M, Huba J, Joyce GC, Huang C (2006) Simulation study of a positive ionospheric storm phase observed at Millstone Hill. Geophys Res Lett 33:L02104. doi:10.1029/2005GL024973

Szuszczewicz EP, Lester M, Wilkinson P, Blanchard P, Abdu M, Hanbaba R, Igarashi K, Pulinets S, Reddy BM (1998) A comparative study of global ionospheric responses to intense magnetic storm conditions. J Geophys Res 103(A6):11665–11684

Tsai LC, Liu CH, Tsai WH, Liu CT (2002) Tomographic imaging of the ionosphere using the GPS/MET and NNSS data. J Atmos Solar Terr Phys 64:2003–2011

Tsurutani B, Mannucci A, Iijima B, Ali Abdu M, Sobral J, Gonzalez W, Guarnieri F, Tsuda T, Saito A, Yumoto K, Fejer B, Fuller-Rowell T, Kozyra J, Foster J, Coster A, Vasyliunas V (2004) Global dayside ionospheric uplift and enhancement associated with interplanetary electric fields. J Geophys Res 109:A08302. doi:10.1029/2003JA010342

Wall ME, Dyck PA, Brettin TS (2001) SVDMAN—singular value decomposition analysis of microarray data. Bioinformatics 17:566–568

Yamamoto A, Ohta Y, Okuzawa T, Taguchi S, Tomizawa I, Shibata T (2000) Characteristics of TEC variations observed at Chofu for geomagnetic storms. Earth Planets Space 52:1073–1076

Yin P, Mitchell CN, Spencer PS, Foster JC (2004) Ionospheric electron concentration imaging using GPS over the USA during the storm of July 2000. Geophys Res Lett 31:L12806. doi:10.1029/2004GL019899